# Island shapes, island densities, and stacking-fault formation on Ir(111): Kinetic Monte Carlo simulations and experiments

Michael Müller* and Karsten Albe
*Institut Für Materialwissenschaft, Technische Universität Darmstadt, D-64287 Darmstadt, Germany*

Carsten Busse,† Arne Thoma, and Thomas Michely
*I. Physikalisches Institut, RWTH Aachen, D-52056 Aachen, Germany*

(Received 5 October 2004; revised manuscript received 16 November 2004; published 18 February 2005)

Submonolayer homoepitaxy on Ir(111) is studied by a refined kinetic lattice Monte Carlo (KLMC) model and compared to results obtained from scanning tunneling microscopy experiments. The KLMC model not only considers individual atomic jumps on regular and stacking-fault sites, but also describes the cooperative motion of small adatom clusters, which determines the temperature-dependent probability of stacking-fault island formation. A complete catalog of diffusion processes at island edges is included that allows one to model the variations of island shapes with temperature. By taking input parameters for cluster and edge diffusion from experiments, calculated island densities as well as the probability of stacking-fault formation agree very well with experimental results for different temperatures. The comparison of simulated and experimental island shapes, however, reveals obvious differences. After systematic modifications of the event database for edge diffusion processes, all features of island shape evolution are well reproduced.

DOI: 10.1103/PhysRevB.71.075407 PACS number(s): 61.72.Nn, 68.55.Ac, 68.35.Fx, 68.37.Ef

## I. INTRODUCTION

During epitaxial growth on (111) surfaces of face-centered cubic (fcc) metals, an important defect is the formation of stacking faults, i.e., the nucleation of adatom islands in hexagonal close-packed (hcp) binding sites, which causes a deviation from the perfect *ABC* stacking sequence to a faulted *ABAB* stacking (compare Fig. 1). The occurrence of stacking faults has a significant influence on the properties of the growing film. A prominent example is the epitaxial growth of Co/Cu multilayers on Cu(111), where the formation of Co islands in hcp instead of fcc adsorption sites leads to a destruction of the desired magnetic properties of the layer system.[1]

Recently, an atomistic description of stacking-fault formation was provided based on experiments on Ir(111).[2] It was found that the probability of stacking-fault formation depends on the diffusivity of adatom clusters. It is determined by the probability that the largest mobile clusters reside in hcp sites. By further attachment of adatoms the clusters are then immobilized and islands grow in a fixed stacking sequence.

In this paper, we present details of a refined kinetic lattice Monte Carlo (KLMC) model for simulations of homoepitaxial growth on fcc(111) surfaces. By allowing adatoms to occupy regular fcc as well as faulted hcp sites, the formation of stacking faults on Ir(111) is simulated. Furthermore, not only individual atomic jumps are considered, but also the cooperative motion of small adatom clusters. Based on these additional features the KLMC model is able to reproduce the temperature dependence of the stacking-fault probability as determined experimentally and therefore gives full support for the atomistic picture presented in Ref. 2.

Mechanisms of cluster diffusion, which cannot be understood as simple sequences of single atomic jumps, have been reported for several metal surfaces in the past (see, e.g., Ref. 3). In KLMC simulations of homoepitaxial thin film growth, however, these cooperative processes have widely been ignored and examples of their influence on macroscopic properties like island densities[4] are still rare. In general it is a challenging task to set up a complete event database for a specific material system, which is required for realistic growth simulations using the KLMC method. In the present study, we therefore took advantage of the extensive amount of experimental data for Ir(111) measured by Ehrlich and co-workers[5–8] and by Tsong and co-workers,[9–11] who carefully investigated the dynamics of Ir adatoms and clusters by field ion microscopy. KLMC simulations based on an event catalog constructed from these experimental data should in principle deliver a consistent description of the island formation processes. While excellent agreement with experiment is

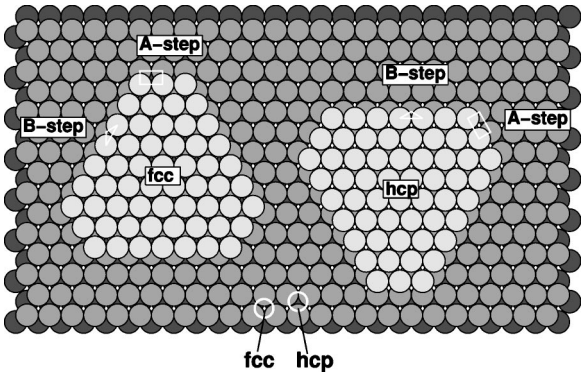


FIG. 1. Ball model of the fcc(111) surface. The figure shows two adatom islands nucleated on regular (fcc) and stacking-fault (hcp) sites, respectively, both bounded predominantly by *B* steps. In order to achieve equivalent step geometry, hcp islands are rotated by 180° with respect to fcc islands.

 

TABLE I. Parameters for Ir clusters of size $i$ on Ir(111). Left hand side: diffusion barrier $E_{d,i}$ and attempt frequency $v_{0,i}$; difference in binding energy $\Delta E_{b,i}=E_{b,i}^{fcc}-E_{b,i}^{hcp}$, binding entropy $\Delta S_{b,i}=S_{b,i}^{fcc}-S_{b,i}^{hcp}$, and free energy $\Delta F_{b,i}=F_{b,i}^{fcc}-F_{b,i}^{hcp}$, between fcc and hcp clusters. Right hand side: Effective energy barriers $E_{d,i}$ and effective attempt frequencies $\nu_{0,i}$ used in the KLMC simulations for transitions of a whole cluster of size $i$ from fcc to hcp binding sites and vice versa. The values are derived from the data given on the left as described in the text (see Sec. III B).

| | Experimental data | | | | | KMC parameters | | | |
|---|---|---|---|---|---|---|---|---|---|
| $i$ | $E_{d,i}$ (eV) | $\nu_{0,i}$ ($s^{-1}$) | $\Delta E_{b,i}$ (eV) | $\Delta S_{b,i}$ ($k_B$) | $\Delta F_{b,i}$ (eV) | $E_{d,i}^{f\to h}$ (eV) | $\nu_{0,i}^{f\to h}$ ($s^{-1}$) | $E_{d,i}^{h\to f}$ (eV) | $\nu_{0,i}^{h\to f}$ (1/s) |
| 1 | 0.290 (Ref. 6) | $2.1\times10^{12}$ (Ref. 6) | 0.023 (Refs. 8 and 15) | 0.64 (Ref. 8) | 0.017 | 0.267 | $1.5\times10^{12}$ | 0.290 | $2.7\times10^{12}$ |
| 2 | 0.447 (Refs. 7 and 15) | $1.4\times10^{11}$ (Refs. 7 and 15) | | | 0.0056 | 0.441 | $1.4\times10^{11}$ | 0.447 | $1.4\times10^{11}$ |
| 3 | 0.646 (Refs. 7 and 15) | $2.3\times10^{12}$ (Refs. 7 and 15) | | | 0 | 0.646 | $2.3\times10^{12}$ | 0.646 | $2.3\times10^{12}$ |
| 4 | 0.477 (Refs. 7 and 15) | $8.2\times10^{10}$ (Ref. 7) | | | -0.031 | 0.477 | $8.2\times10^{10}$ | 0.446 | $8.2\times10^{10}$ |
| 5 | 0.685 (Refs. 7 and 15) | $3.3\times10^{10}$ (Refs. 7 and 15) | | | -0.086 | 0.685 | $3.3\times10^{10}$ | 0.599 | $3.3\times10^{10}$ |

achieved for island densities and stacking-fault probabilities, discrepancies arise regarding the island shapes. We find evidence for inconsistencies in the experimental data and propose a modified potential energy diagram for diffusion along island edges that leads to a very good agreement of simulated and measured island shapes.

## II. EXPERIMENTS

The experiments were performed in an UHV chamber with a base pressure $P<3\times10^{-11}$ mbar. The sample was cleaned by repeated cycles of sputtering and annealing, resulting in a clean surface and a terrace width of several 1000 Å. Prior to deposition the sample was flashed to a temperature ensuring desorption of all species that might have adsorbed from the background gas. Ir was evaporated with a standard deposition rate of $F=1.3\times10^{-2}$ monolayers (ML)/s from a resistance-heated wire. Special care was exercised to ensure clean deposition conditions ($P<1\times10^{-10}$ mbar). After deposition the sample was quenched to avoid changes of island shapes. The resulting morphology was analyzed by variable temperature scanning tunneling microscopy (STM).

## III. KLMC MODEL

In the past, island nucleation as well as homoepitaxial thin film growth have been successfully studied by means of kinetic Monte Carlo schemes using solid-on-solid models that allow for atomic jumps on ideal lattice sites. For studying the case of stacking-fault nucleation, we developed a code with two additional features, namely, stacking faults and cluster diffusion by cooperative motion, which is described in detail in this section.

### A. Refined lattice

As illustrated in Fig. 1, adatoms on a fcc(111) surface can occupy two kinds of nonequivalent adsorption sites, namely, regular sites corresponding to a fcc stacking sequence (*ABC*) and irregular sites that introduce a faulted, hcp stacking sequence (*ABAB*). STM studies of Ir(111) homoepitaxy revealed that a significant fraction of adatom islands nucleate in the faulted stacking. At temperatures below 230 K the stacking-fault islands are even predominant.[2] In order to implement the formation of stacking faults in a lattice Monte Carlo model, adatoms must be allowed to occupy regular fcc as well as hcp sites. This is achieved by using a refined fcc lattice with additional sites at all possible stacking-fault positions. On this lattice, terrace diffusion of adatoms is described by jumps of an atom from a fcc binding site to one of the three neighboring hcp binding sites and vice versa.

### B. Cluster diffusion

The detailed diffusion mechanisms of adatom clusters can be very complex, consisting of numerous single-atom and concerted motion mechanisms,[3,5,6,12–14] and therefore cannot be simply mimicked by a sequence of individual atomic jumps. For clusters on Ir(111), diffusion processes are described in some detail in Ref. 7, but there are not enough data available to deduce all attempt frequencies and energy barriers. However, for the phenomena studied here, one is only interested in correctly reproducing the time intervals a cluster spends in fcc or hcp binding sites. Therefore, the detailed diffusion mechanisms can be neglected and cluster diffusion can be described in a coarse grained way: Clusters are treated as nonrotatable objects that diffuse as a whole by jumps from fcc to hcp binding sites and vice versa. Also, no distinction is made between compact clusters and chains of atoms. We consider temperatures up to 400 K, where pentamers are the largest mobile clusters. Therefore, diffusion of larger clusters can be neglected. In order to determine the rates of the processes $\nu_i^{f\to h}$ (jump of a cluster of size $i$ from fcc to hcp) and $\nu_i^{h\to f}$ (vice versa), we employ effective attempt frequencies ($\nu_{0,i}^{f\to h}$, $\nu_{0,i}^{h\to f}$) and effective energy barriers ($E_{d,i}^{f\to h}$, $E_{d,i}^{h\to f}$). The values of these parameters are derived from FIM data on diffusion barriers $E_{d,i}$, attempt frequencies $\nu_{0,i}$, and differences in free binding energy $\Delta F_{b,i}$ and binding entropy $\Delta S_{b,i}$ between fcc and hcp sites for Ir clusters on Ir(111).[6–8] A complete summary of the field ion microscopy (FIM) data is given in Ref. 2; the left hand side of Table I lists the data relevant for the present work. For clusters larger than monomers, $\Delta S_{b,i}$ is not known and we obtain the effective attempt frequencies by approximating $\nu_{0,i}^{f\to h}=\nu_{0,i}^{h\to f}=\nu_{0,i}$. For monomers, $\Delta S_{b,i}$ is included in the effective attempt frequencies by setting

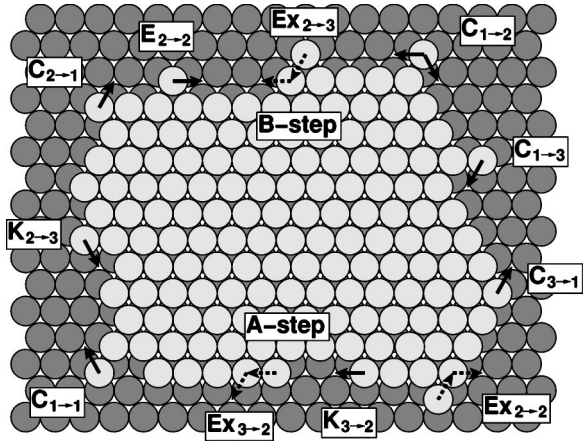


FIG. 2. Illustration of the diffusion processes at island edges implemented in our KLMC model. The notation is adopted from Ref. 18: The letters denote corner, edge, kink, and exchange; the subscripts give the in-layer coordination numbers before and after the process. All processes can take place at *A* and *B* steps of regular as well as stacking-fault islands.

$$\nu_{0,1}^{\mathrm{f}\to\mathrm{h}} = \nu_{0,1} \times \frac{2}{1+\exp(\Delta S_{\mathrm{b},1}/k_{\mathrm{B}})} \tag{1}$$

and

$$\nu_{0,1}^{\mathrm{h}\to\mathrm{f}} = \nu_{0,1} \times \frac{2}{1+\exp(-\Delta S_{\mathrm{b},1}/k_{\mathrm{B}})}, \tag{2}$$

with $\nu_{0,1}$ and $\Delta S_{\mathrm{b},1}$ from Table I. Equations (1) and (2) ensure that $(\nu_{0,1}^{\mathrm{f}\to\mathrm{h}}+\nu_{0,1}^{\mathrm{h}\to\mathrm{f}})/2=\nu_{0,1}$. The rate-limiting energy barrier $\max\{E_{\mathrm{d},i}^{\mathrm{f}\to\mathrm{h}}, E_{\mathrm{d},i}^{\mathrm{h}\to\mathrm{f}}\}$ of the two inequivalent hops is approximated by the diffusion barrier $E_{\mathrm{d},i}$. In order to satisfy the condition of detailed balance, the other diffusion barrier $\min\{E_{\mathrm{d},i}^{\mathrm{f}\to\mathrm{h}}, E_{\mathrm{d},i}^{\mathrm{h}\to\mathrm{f}}\}$ must then be equal to $E_{\mathrm{d},i}-|\Delta E_{\mathrm{b},i}|$, where $\Delta E_{\mathrm{b},i}$ is the difference in binding energy between fcc and hcp clusters. For monomers, this binding energy difference is obtained by $\Delta E_{\mathrm{b},1}=\Delta F_{\mathrm{b},1}+T_{\mathrm{m}}\Delta S_{\mathrm{b},1}$($T_{\mathrm{m}}=106$ K, the temperature at which $\Delta F_{\mathrm{b},1}$ and $\Delta S_{\mathrm{b},1}$ have been determined[8]). For larger clusters, $\Delta S_{\mathrm{b},i}$ is not known, and $\Delta E_{\mathrm{b},i}$ is approximated by $\Delta F_{\mathrm{b},i}$. The resultant cluster diffusion parameters are listed on the right hand side of Table I.

### C. Diffusion at island edges

In contrast to terrace diffusion, diffusion of atoms bound to island edges is implemented by jumps from fcc to fcc sites, if the whole island is nucleated on fcc sites. If the island is nucleated on hcp sites, jumps are from hcp to hcp. A vast amount of diffusion processes at island edges can be distinguished, as depicted in Fig. 2. Their influence on the kinetically controlled island shape has already been investigated in a number of KLMC simulations.[16–20] An overview of island shapes can be found in Ref. 22. High diffusivity at island edges leads to the formation of compact islands surrounded by close-packed steps. On a fcc(111) surface, two different kinds of close-packed steps exist, namely, the {100}-microfaceted *A* steps and the {111}-microfaceted *B* steps (for an illustration see Fig. 1). For many fcc(111) surfaces, an anisotropy in free energy of these two step types exists, leading to anisotropic potential energy landscapes for diffusion along the island edges.[21] In most cases, this results in preferential growth of *A* steps and islands with a triangular envelope evolve, bounded predominantly by the more slowly growing *B* steps.[22] If the diffusivity at island edges is reduced, ramified fractal islands are formed. Again, anisotropic diffusion will lead to triangular islands, as the branches exhibit preferred growth directions perpendicular to either *A* or *B* steps.[20] Fractal islands with preferential growth directions are commonly referred to as dendritic islands.

For describing the features of shape evolution during island growth, all processes shown in Fig. 2 are distinguished in our KLMC model. We determine the activation energies for these processes by constructing a potential energy diagram of diffusion around island steps on Ir(111) based on the following experimental data and observations. On Ir(111), the *B* steps possess a lower step free energy than *A* steps.[21] As an effect, an extra atom at a densely packed step is bound more strongly to an *A* than to a *B* step. By field ion microscopy, Fu *et al.* estimated the difference in binding energy $\delta_{AB}$ to be at least 0.21 eV.[10] They also determined the activation energies for diffusion along straight *A* and *B* steps ($\mathrm{E}_{2\to2}$ in Fig. 2: 0.82 and 0.76 eV, respectively).[10] Furthermore, they found an anisotropy for diffusion from a corner site toward an *A* or *B* step ($\mathrm{C}_{1\to2}$): The activation energy of a jump toward a *B* step is 0.04 eV higher than the activation energy of a jump toward an *A* step, which they found to be 0.36 eV.[11] From the observation that even at high temperatures no atoms detach from the islands during diffusion around the corner from one step to a neighboring step, they conclude that atoms diffuse around the corner via an exchange mechanism ($\mathrm{Ex}_{2\to2}$), avoiding the only onefold coordinated corner site position with the small binding energy.[11] From the given onset temperature for diffusion around the corner from *A* to *B* steps (350 K) and from *B* to *A* steps (260 K), one can deduce the activation energies for these processes to be 0.93 and 0.69 eV, respectively. The dimer binding energy $E_{\mathrm{b},2}$ on Ir(111), which allows one to estimate the binding energy difference for atoms attached to corners, edges, and kinks, has been determined by STM ($E_{\mathrm{b},2}=0.88$ eV for a diffusion prefactor of $1.1\times10^{13}$ s$^{-1}$).[23]

From these data, we construct a potential energy diagram by using a simple nearest-neighbor model, where all processes with the same initial and saddle point nearest-neighbor configurations possess the same activation energy. In this nearest-neighbor model, it is consequent to assume that exchange processes are also active for diffusion around kinks ($\mathrm{Ex}_{2\to3}$ and $\mathrm{Ex}_{3\to2}$), since the configurations of $\mathrm{Ex}_{2\to3}$ and $\mathrm{Ex}_{2\to2}$ are identical within the nearest-neighbor distance. Satisfying the detailed balance criterion, the difference between the activation energies of processes $\mathrm{Ex}_{2\to2}^{\mathrm{A}}$ and $\mathrm{Ex}_{2\to2}^{\mathrm{B}}$ must equal $\delta_{\mathrm{AB}}$, which gives $\delta_{\mathrm{AB}}=0.24$ eV, in good agreement with the experimentally determined value of $\delta_{\mathrm{AB}} \geqslant 0.21$ eV. The differences in binding energy for one-, two-, and three-fold coordinated atoms at *A* and *B* steps are set to values consistent with $E_{\mathrm{b},2}$ and $\delta_{\mathrm{AB}}$: Because of the embedding effect, the difference between the binding energy at a corner site and the binding energy at an edge site $\Delta E_{1,2}$ must

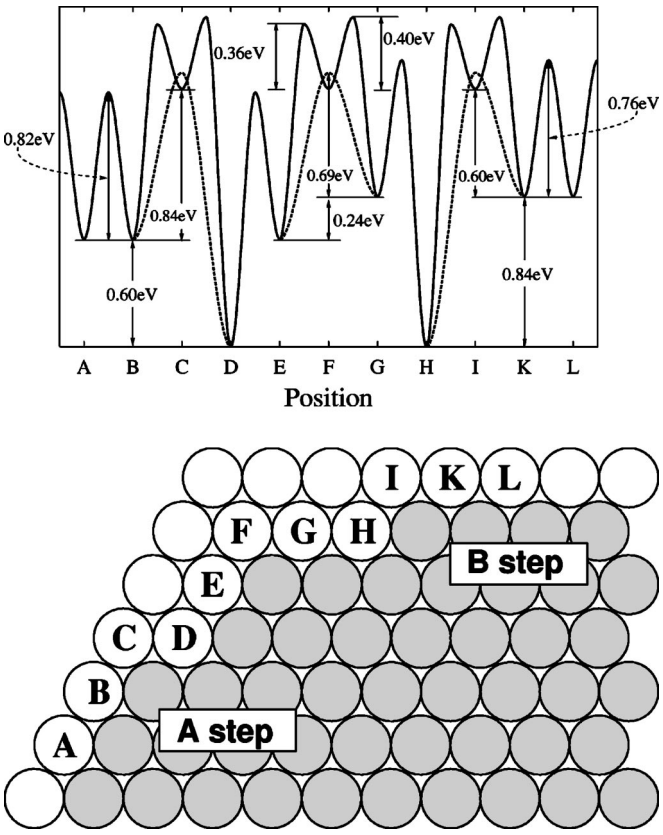


FIG. 3. Potential energy diagram for adatom diffusion along fcc island edges, as derived from a nearest-neighbor model using experimental data as input parameters (see text). Solid lines denote energy paths for diffusion via hopping processes, dashed lines energy paths for diffusion via exchange mechanisms. The potential energy diagram for diffusion along hcp island edges is obtained by raising all energy minima by 0.08 eV and keeping the saddle point energies fixed (see text).

be smaller, but still in the order of $E_{b,2}$. We choose $\Delta E_{1,2}=0.84$ eV for the *A* step. Using again $\delta_{AB}=0.24$ eV we obtain $\Delta E_{1,2}=0.60$ eV for the *B* step. Since nothing is known about a difference between the binding energies at kink sites on *A* and *B* steps, we set them both to equal values. The resulting potential energy diagram for diffusion at fcc island edges is shown in Fig. 3, the corresponding activation energies are listed in Table II.

For diffusion at hcp island edges, a modified catalog of activation energies is used. The excess energy of an entire stacking-fault layer is about 0.08 eV.[24] One can now assume that the binding energy of an atom in a potential energy minimum at the edge of a hcp island is lowered by the same amount compared to an atom at a fcc island. In contrast, the energy of the saddle point of a diffusion process should only weakly depend on the island type. Therefore, all activation energies of diffusion processes at hcp islands are reduced by 0.08 eV with respect to the diffusion processes at fcc islands.

For all processes at island edges, the diffusion prefactor $\nu_0$ is set to $2\times10^{12}$ s$^{-1}$, which is consistent with the prefactor $D_0=10^{-3}$ cm$^2$/s used by Fu *et al.* for the determination of activation energies from FIM.[11]

Atoms that are deposited on top of already existing islands are treated the same way as atoms in the first monolayer. Since in the experiments a pure layer-by-layer growth mode has been observed, these atoms can cross the island edges with no additional barrier and will therefore be incorporated in the first monolayer.

TABLE II. Activation energies for diffusion processes at island edges, as derived from the potential energy diagram in Fig. 3. The notation of these processes is described in Fig. 2.

| | Activation energy (eV) | | | |
|---|---|---|---|---|
| | fcc island | | hcp island | |
| Process | *A* step | *B* step | *A* step | *B* step |
| $C_{1\to1}$ | 0.36 | 0.40 | 0.28 | 0.32 |
| $C_{1\to2}$ | 0.36[a] | 0.40[a] | 0.28 | 0.32 |
| $C_{1\to3}$ | 0.40 | 0.36 | 0.32 | 0.28 |
| $C_{2\to1}$ | 1.20 | 1.00 | 1.12 | 0.92 |
| $C_{3\to1}$ | 1.84 | 1.80 | 1.76 | 1.72 |
| $E_{2\to2}$ | 0.82[a] | 0.76[a] | 0.74 | 0.68 |
| $K_{2\to3}$ | 0.82 | 0.76 | 0.74 | 0.68 |
| $K_{3\to2}$ | 1.42 | 1.60 | 1.34 | 1.52 |
| $Ex_{2\to2}$ | 0.93[a] | 0.69[a] | 0.85 | 0.61 |
| $Ex_{2\to3}$ | 0.93 | 0.69 | 0.85 | 0.61 |
| $Ex_{3\to2}$ | 1.53 | 1.53 | 1.45 | 1.45 |

[a]Reference 11.

## IV. SIMULATIONS AND RESULTS

### A. Island density and stacking-fault probability

For the studies on island density and stacking-fault probability, we simulated Ir island nucleation on Ir(111) in a temperature regime from 125 to 400 K. Atoms have been deposited at random sites on the surface with a deposition rate of $F=1.3\times10^{-2}$ ML/s. The simulation time was 10 s, resulting in a final coverage of 0.13 ML. In order to achieve good statistics, the dimensions of the surface had to be chosen large enough (from $1000\times1000$ Å$^2$ for low temperatures up to $1500\times1500$ Å$^2$ for the highest temperatures) to guarantee the formation of a sufficient number of islands. In Fig. 4, the island densities [expressed by the saturation island density $n_{sat}$=(number of islands/number of sites) obtained from our simulations are compared to the experimental island densities.[23]

The temperature dependence of the stacking-fault island probability as obtained from our KLMC model is shown in Fig. 5. For comparison, the experimental results from Ref. 2 were used, where the probability of stacking-fault formation was explained by a simple atomistic model based on the diffusion behavior of small adatom clusters: If at a given temperature clusters of size *i* are the largest mobile clusters that contribute effectively to the surface diffusion, then the ratio of regular to faulted islands $N_{hcp}/N_{fcc}$ is governed by the ratio of the average resident times in the hcp and fcc adsorption sites, because by attachment of another adatom the cluster is immobilized.

The agreement between experiment and simulation in both island density and stacking-fault island probability that

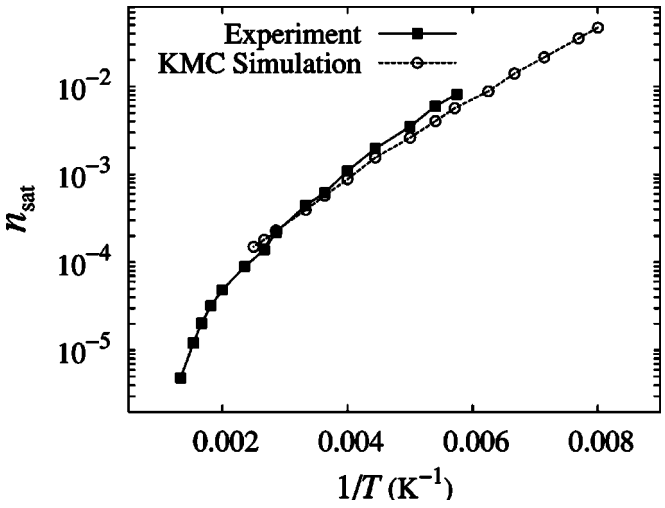


FIG. 4. Island densities as obtained by experiment and KLMC simulation with a deposition rate of 0.013 ML/s and a coverage of 0.13 ML.

our model reproduces all processes relevant for the formation of stacking-fault islands in the system Ir/Ir(111) and confirms that our coarse grained description of cluster diffusion is adequate. Furthermore, it strongly supports the rate-equation approach developed in Ref. 2. The good agreement between the measurements and simulations with input from independent experiments also rules out the presence of contaminations in the STM study.

From the methodical point of view, these results demonstrate the importance of including concerted motion mechanisms in a KLMC event catalog: With cluster diffusion suppressed, the relative stacking-fault probability would be determined by monomer diffusion alone and would therefore tend toward the ratio $\nu_{0,1}^{f\to h}/\nu_{0,1}^{f\to h}\approx 0.556$ with increasing temperature, instead of continually decreasing toward zero. Also, cluster diffusion influences the island density. The mobility of larger adatom entities leads to a reduction of island densities compared to the case where single atoms diffuse exclusively.[4,25]

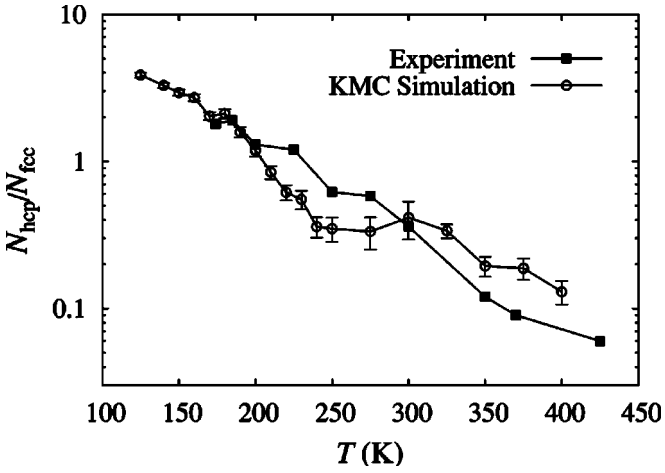


FIG. 5. Temperature dependence of the stacking-fault island probability $N_{hcp}/N_{fcc}$ on Ir(111) as obtained by experiment and KLMC simulation.

### B. Island shapes

In order to compare experimental and simulated island shapes over a wider temperature range, we also performed simulations at 450, 500, and 600 K. At these high temperatures also larger clusters like hexamers and heptamers become mobile.[2] Since we only include cluster diffusion for sizes up to pentamers, island densities and stacking-fault probabilities are too large in the simulations at these temperature. The island density, for example, is about twice the experimental value for the highest temperature considered. In Fig. 6, we compare the experimentally observed island shapes (first column) with those obtained from KLMC simulations (second column), using the activation energies given in Table II. In the experiments, dendritic islands with a triangular envelope bounded predominantly by *B* steps are found at 250 and 375 K. At higher temperatures, a transition from dendritic to compact islands with broad arms perpendicular to *A* steps can be observed. At 450 K, one can clearly see that stacking-fault islands develop smoother edges than regular islands, which is due to the reduced binding energy of atoms at stacking-fault islands, as discussed in Sec. III C. This effect can also be observed at 375 K. The regions shown in the images at 500 and 600 K do not feature any stacking-fault islands.

The simulations reproduce the transition from fractal to compact islands and the triangular shape at higher temperatures. However, they clearly deviate from the experimental observations in the following points: At 250 K, the simulated islands exhibit almost no preferential growth directions, most of the islands are isotropic and possess no triangular envelope. Also, the transition from fractal to compact islands occurs at much lower temperatures: At 375 K, the island shape is already in an intermediate state between fractal and compact. The islands at 450, 500, and 600 K are almost perfect compact triangles.

With all other diffusion processes at island edges almost frozen in, the only active processes at 250 K are $C_{1\to 1}$, $C_{1\to 2}$, and $C_{1\to 3}$ (corner processes) and a preferential growth direction can only arise from a difference of the activation energies of these processes toward *A* and *B* steps. Therefore, the loss of preferential growth directions at 250 K in the KLMC simulations signifies that the anisotropy of the corner processes of only 0.04 eV (i.e., the difference between $C_{1\to 2}^{A}$ and $C_{1\to 2}^{B}$) is too low. Furthermore, the shift of the transition from fractal to compact islands to much lower temperatures indicates that the mobility of atoms at island edges is generally too high in our model.

In order to improve the agreement between simulations and experiments, we increased the anisotropy of the corner jumps to 0.1 eV. We also decreased the mobility of atoms at island edges by increasing all activation energies listed in Table II according to the following procedure. The activation energies in Ref. 11 are given by $E_a = 2.6\times 10^{-3}$ eV/K$\times T$, where $T$ is the experimentally determined onset temperature for the diffusion process of interest. If one assumes an offset $\Delta T$ in the temperature calibration of the experiments, it follows that all activation energies listed in Table II have to be increased by $2.6\times 10^{-3}$ eV/K$\times\Delta T$. We examined the effect of various temperature offsets and found a very good agree-

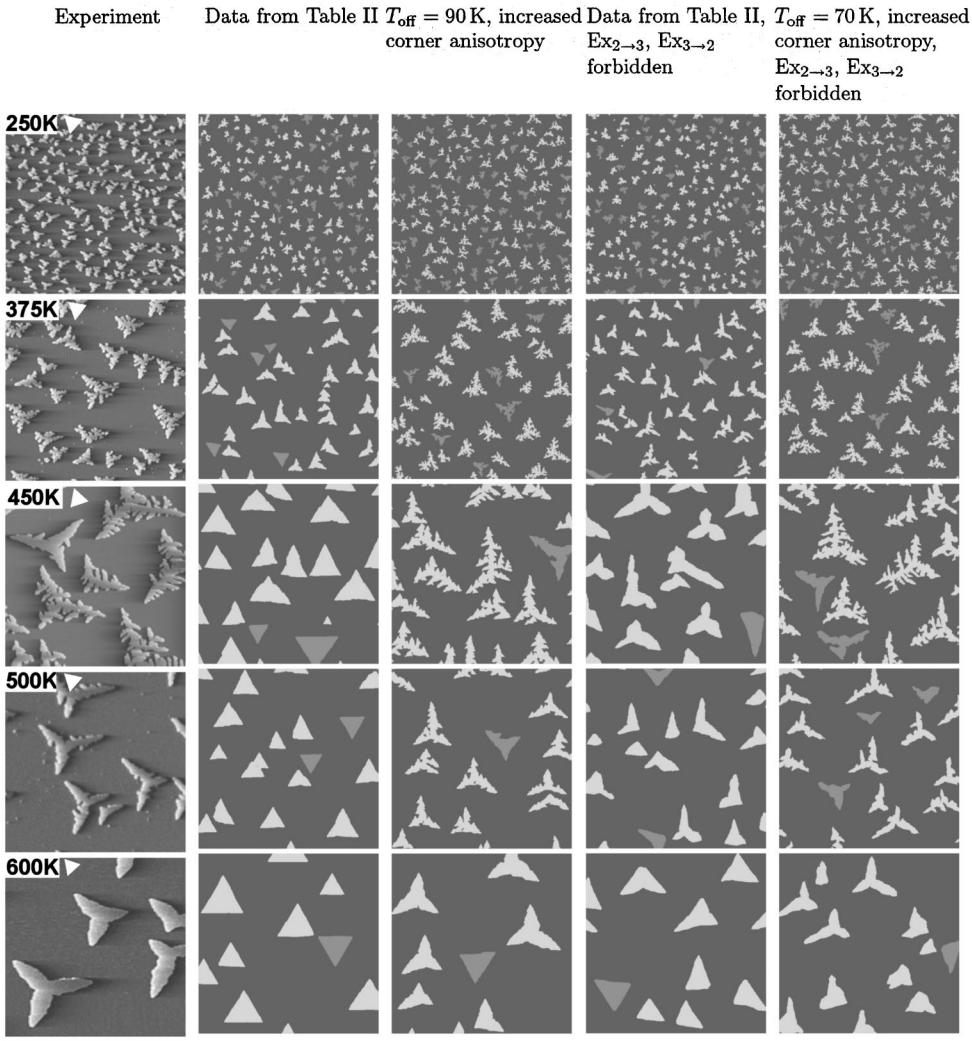


FIG. 6. Island shapes after deposition of 0.13 ML of Ir on Ir(111) with a deposition rate of $1.3\times10^{-2}$ ML/s (250, 375, 500, and 600 K) and after deposition of 0.22 ML with a deposition rate of $4.9\times10^{-3}$ ML/s (450 K). First column: STM topographs. Second column: KLMC simulations using the activation barriers listed in Table II. Third column: KLMC simulations with activation energies increased according to a temperature offset of 90 K and increased corner anisotropy (see potential energy diagram Fig. 7). Fourth column: KLMC simulations using the activation barriers listed in Table II, processes $Ex_{2\to3}$ and $Ex_{3\to2}$ forbidden. Fifth column: KLMC simulations with increased activation energies according to a temperature offset of 70 K, increased corner anisotropy, and processes $Ex_{2\to3}$ and $Ex_{3\to2}$ forbidden. The picture size is $1200\times1200$ Å$^2$. In column 1, the orientation of regular islands is indicated by white triangles. In columns 2 to 5, regular islands are colored light gray, stacking-fault islands dark gray.

ment between simulations and experiments for $\Delta T=90$ K, as shown in the third column of Fig. 6. The increased corner jump anisotropy now leads to the formation of triangular shaped islands at 250 K. Also, the increase of all activation energies shifts the transition from fractal to compact islands to higher temperatures, reproducing the dendritic shape at 450 K, the intermediate shape at 500 K, and the triangles with broad arms at 600 K. The potential energy diagram for diffusion at island edges including the modifications described above is shown in Fig. 7. We verified that the island densities and stacking-fault probabilities are not influenced significantly by the rescaled barriers.

One might argue that the compact shape of the islands in the simulations with no temperature offset is due to the kink exchange processes ($Ex_{2\to3}$ and $Ex_{3\to2}$), since the process $Ex_{2\to3}$ renders an incorporation of edge atoms into kinks very likely and therefore efficiently causes the islands to develop smooth edges. As described in Sec. III C, the kink exchange processes have been included in the event catalog in consistency with the nearest-neighbor model. However, no experimental evidence either for or against diffusion around kinks via exchange mechanisms exists in the system Ir/Ir(111). In order to examine the influence of kink exchange processes on the island shape, we also performed simulations using the initial potential energy diagram (Fig. 3), but suppressing the kink exchange processes. The results of these simulations are shown in the fourth column of Fig. 6. Comparing them to the shapes of the islands obtained with the initial potential energy diagram (Fig. 6, column 2), one can observe that the suppression of kink exchange processes indeed reduces the compactness of the islands visibly. However, in order to obtain a qualitative agreement of simula-

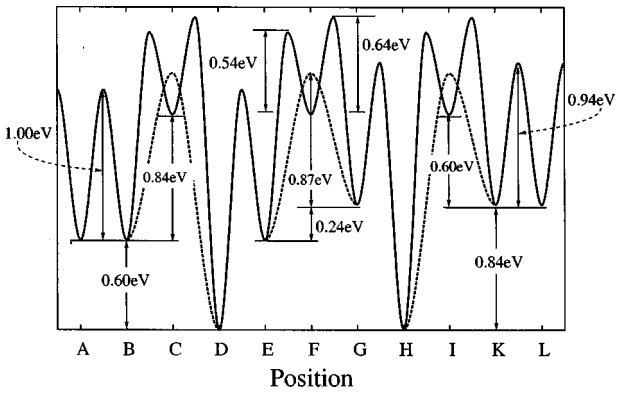


FIG. 7. Modified potential energy diagram for adatom diffusion along fcc island edges, with increased activation barriers and increased corner anisotropy. Positions are the same as in Fig. 3.

tions and experiments a temperature offset of $\Delta T = 70$ K and an increased corner anisotropy has to be assumed also for the case of suppressed kink exchange processes. This is demonstrated in the fifth row of Fig. 6.

Starting from the diagram in Fig. 7, an even better agreement between simulations and experiment could be achieved by adjusting all activation energies independently from each other. However, because of the large number of parameters, finding one good fit is no guarantee that no other parameter sets exist that produce equally good or even better results and would therefore be of only minor relevance.

Finally, it should be noted that the modified catalog of activation energies for hcp islands—namely the reduction of the edge diffusion energy barriers by the stacking-fault energy per atom—adequately reproduces the experimentally observed more compact stacking-fault island shapes. This is apparent by comparison of the experimental data for 375 and 450 K with the corresponding simulation data with temperature offset (third and fifth columns of Fig. 6). This proves an enhanced step edge diffusion along stacking-fault islands. At higher coverages the reduced binding energy of corner and kink atoms at stacking-fault islands is supposed to be the decisive factor in the effective assimilation of hcp islands by fcc islands upon coalescence.[26] At higher temperatures the weaker binding of edge atoms might also lead to a preferential two-dimensional ripening of stacking-fault islands by atom detachment.

## V. DISCUSSION

The comparison of island shapes from KLMC simulations and experiment reveals discrepancies between the presently available experimental data on edge diffusion on the one hand and experimentally observed island shapes on the other hand. The simulations show that the activation energies obtained from FIM experiments overestimate the mobility of atoms at island edges. A possible cause for this discrepancy can be the temperature calibration of the experimental setup. This explanation is supported by different values published for the adatom diffusion barrier on Ir(111) obtained by FIM studies: On the basis of a precise temperature calibration, Wang and Ehrlich report a value of 0.29 eV for the adatom diffusion barrier,[6] while the value reported by Chen and Tsong for the same process is 0.22 eV.[9] This would point to a temperature offset of $\approx 30$ K, so an offset alone cannot lift the discrepancy.

Another reason can be an island size dependence of activation energies. For example, for Pt(111), evidence from density functional calculations exists that diffusion of an atom along straight steps far away from a corner is different from diffusion along a straight step close to a corner.[28] A further theoretical proof of a strong size dependence of activation energies and diffusion mechanisms can be found in Ref. 27. The islands in the FIM studies are limited to sizes of less than a hundred atoms,[10] while the islands observed in the present study consist of several thousand atoms.

Finally, it should be noted that although our model accounts for a large number of diffusion processes at island edges, the possibility of omitting an important mechanism in the event catalog can never be ruled out. Therefore, it is possible that a fraction of the observed temperature offset is due to some missing process in the KLMC model.

From the comparison of island shapes from KLMC simulations and experiment at 250 K, we conclude that the experimentally determined corner anisotropy of only 0.04 eV is too small to explain the triangular shaped islands at low temperatures. This may mean either that the corner anisotropy is in fact higher than the measured value, or that other processes, which are not included in our KLMC model, also contribute to the preferential growth of *A* steps. In the latter case, the value for the anisotropy used in the KLMC simulations is to be considered as a free parameter that can be adjusted to reproduce the experimental results. In the following, processes that can also lead to a preferred growth direction and that are not included in our KLMC model are discussed.

The anisotropy has only been measured for the $C_{1\rightarrow 2}$ process. Therefore, this anisotropy can be different for the $C_{1\rightarrow 1}$ and $C_{1\rightarrow 3}$ processes, while, according to the nearest-neighbor model of our simulations, the anisotropy was set to the same value for all corner processes. However, in order to cause the formation of triangular islands, the difference would have to be very large, which seems very unlikely.

Another effect that cannot be included in a simple nearest-neighbor model has been suggested in Ref. 20. In summary, it is proposed that the potential energy landscape of an adatom approaching a fcc (hcp) island via a hcp (fcc) site is already influenced by the presence of the nearby adatom island. In consequence, if the adatom approaches an *A* step, it is more likely to attach to a twofold coordinated site than to a onefold coordinated site, while no preference exists if the adatom approaches a *B* step. Consequently, this effect can also lead to a preferred growth of *A* steps, independent from corner anisotropies. However, we note that Fu *et al.* frequently observed the attachment of adatoms at island corners.[11] Therefore, this effect seems to play only a minor role in the system Ir/Ir(111).

Finally, Wang and Ehrlich show that on Ir(111), an attractive interaction between steps and adatoms over a few nearest-neighbor distances exists.[29] Since atoms are bound more strongly to *A* steps, the attraction between adatoms and

*A* steps may be stronger than the attraction between adatoms and *B* steps. Again, the effect would be a preferred growth of *A* steps.

## VI. CONCLUSIONS

In summary, a KLMC model of stacking-fault island formation on Ir(111) is presented that implements a refined lattice for the representation of stacking-fault sites and that explicitly includes the diffusion of small adatom clusters. By using experimentally determined cluster diffusion parameters, this model accurately reproduces the experimentally observed temperature dependence of the island density as well as the stacking-fault probability. The present simulations show the importance of cluster diffusion and concerted motion processes for simulating stacking-fault formation on Ir(111). In general, these results suggest that cooperative atomic motion might also be of importance in other material systems and therefore should not be neglected in KLMC simulations. The comparison of experimental island shapes with those obtained by KLMC simulations shows that the presently available experimental data on edge diffusion cannot explain all features of island shape observed in Ir(111) homoepitaxy. The small corner anisotropy leads to a lack of pronounced triangular islands at low temperatures. The transition from fractal to compact islands occurs at too low temperatures, which signifies that the mobility of atoms at island edges is overestimated. Based on these observations, a modified rate catalog with increased corner anisotropy and decreased mobility of atoms at island edges is proposed that leads to a very close accordance between simulations and experiments regarding island shapes. The comparison of the simulated and observed island shapes shows also that the more compact hcp islands are due to a reduction of the edge diffusion activation barriers along hcp islands, which originates from a weaker binding of edge atoms at hcp islands. In order to validate this rate catalog, further experimental or theoretical studies using first principles calculations are desirable.

## ACKNOWLEDGMENT

This work was supported in part by the Deutsche Forschungsgemeinschaft through the project "Atomare Prozesse beim homoepitaktischen Schichtwachstum."

*Electronic address: mueller@mm.tu-darmstadt.de

†Present address: Interdisciplinary Nanoscience Center (iNANO), Center for Atomic Scale Materials Physics (CAMP), and Department of Physics and Astronomy, University of Aarhus, DK-8000 Aarhus C, Denmark.

[1] J. de la Figuera, J. E. Prieto, C. Ocal, and R. Miranda, Phys. Rev. B **47**, 13 043 (1993).

[2] C. Busse, C. Polop, M. Müller, K. Albe, U. Linke, and T. Michely, Phys. Rev. Lett. **91**, 056103 (2003).

[3] J. C. Hamilton, M. S. Daw, and S. M. Foiles, Phys. Rev. Lett. **74**, 2760 (1995).

[4] S. Liu, L. Bönig, and H. Metiu, Phys. Rev. B **52**, 2907 (1995).

[5] U. Kürpick, B. Fricke, and G. Ehrlich, Surf. Sci. Lett. **470**, L45 (2000).

[6] S. C. Wang, U. Kürpick, and G. Ehrlich, Phys. Rev. Lett. **81**, 4923 (1998).

[7] S. C. Wang and G. Ehrlich, Surf. Sci. **239**, 301 (1990).

[8] S. C. Wang and G. Ehrlich, Phys. Rev. Lett. **68**, 1160 (1992).

[9] C. L. Chen and T. T. Tsong, Phys. Rev. B **41**, 12 403 (1990).

[10] T. Y. Fu, Y. R. Tzeng, and T. T. Tsong, Surf. Sci. Lett. **366**, L691 (1996).

[11] T.-Y. Fu and T. T. Tsong, Phys. Rev. B **61**, 4511 (2000).

[12] A. Bogicevic, P. Hyldgaard, G. Wahnström, and B. I. Lundqvist, Phys. Rev. Lett. **81**, 172 (1998).

[13] P. Salo, J. Hirvonen, I. T. Koponen, O. S. Trushin, J. Heinonen, and T. Ala-Nissila, Phys. Rev. B **64**, 161405(R) (2001).

[14] G. Henkelman and H. Jónsson, Phys. Rev. Lett. **90**, 116101 (2003).

[15] G. Ehrlich (private communication).

[16] H. Jónsson, Annu. Rev. Phys. Chem. **51**, 623 (2000).

[17] S. Ovesson, A. Bogicevic, and B. I. Lundqvist, Phys. Rev. Lett. **83**, 2608 (1999).

[18] A. Bogicevic, J. Strömquist, and B. I. Lundqvist, Phys. Rev. Lett. **81**, 637 (1998).

[19] J. Jacobsen, K. W. Jacobsen, and J. K. Nørskov, Surf. Sci. **359**, 37 (1996).

[20] H. Brune, H. Röder, K. Bromann, K. Kern, J. Jacobsen, P. Stoltze, K. Jacobsen, and J. Nørskov, Surf. Sci. Lett. **349**, L115 (1996).

[21] M. J. Rost, T. Michely, and G. Comsa, Phys. Rev. B **57**, 1992 (1998).

[22] T. Michely and J. Krug, *Islands, Mounds and Atoms* (Springer, Berlin, 2003).

[23] C. Busse, W. Langenkamp, C. Polop, A. Petersen, H. Hansen, U. Linke, P. J. Feibelman, and T. Michely, Surf. Sci. Lett. **539**, L560 (2003).

[24] J. C. Hamilton, M. R. Sørensen, and A. F. Voter, Phys. Rev. B **61**, R5125 (2000).

[25] K. Kyuno and G. Ehrlich, Phys. Rev. Lett. **84**, 2658 (2000).

[26] C. Busse and T. Michely, Surf. Sci. **552**, 281 (2004).

[27] F. Montalenti, Surf. Sci. **543**, 141 (2003).

[28] P. J. Feibelman, Phys. Rev. B **60**, 4972 (1999).

[29] S. C. Wang and G. Ehrlich, Phys. Rev. Lett. **70**, 41 (1993).